



Article

Long-Term Spatiotemporal Characteristics and Impact Factors of Land Surface Temperature of Inhabited Islands with Different Urbanization Levels

Junmao Zhang ^{1,2} , Tao Lin ^{1,2,*} , Caige Sun ³ , Meixia Lin ¹ , Yulin Zhan ^{2,4} , Yuan Chen ¹, Hong Ye ^{1,2}, Xia Yao ¹, Yiyi Huang ^{1,5}, Guoqin Zhang ^{1,2} and Yuqin Liu ¹

- ¹ Key Laboratory of Urban Environment and Health, Institute of Urban Environment, Chinese Academy of Sciences, Xiamen 361021, China
² College of Resources and Environment, University of Chinese Academy of Sciences, Beijing 100049, China
³ School of Geography, South China Normal University, Guangzhou 510631, China
⁴ Aerospace Information Research Institute, Chinese Academy of Sciences, Beijing 100094, China
⁵ Coastal and Ocean Management Institute, Xiamen University, Xiamen 361102, China
* Correspondence: tlin@iue.ac.cn

Abstract: Surface thermal environment (STE) is closely related to the comfort and health of residents, affecting regional livability, and its spatial and temporal changes are deeply affected by the urbanization process. Considering there is a lack of effective comparative analysis on STE in different urbanized inhabited islands, the special geographical unit and vital human settlement environment, long-term spatiotemporal characteristics and impact factor quantitative analyses were performed in two inhabited islands via the RS and GIS methods. The results suggest that the surface heat amplitude of the highly urbanized Xiamen Island decreases, with the surface heat intensity continuing to increase from 2000 to 2020, while that of the lowly urbanized Kinmen Island is reversed. Although the land surface temperature (LST) of the two inhabited islands shows similar spatial distribution characteristics with evident cold/hot spots, the geographical distribution characteristics of high LST zones are significantly different, and the thermal landscape of Xiamen Island is more fragmented, discrete, and simple in shape, as revealed by the landscape metrics. We demonstrate that the area proportion between cooling land (water body and greenland) and warming land (bare land and impervious surface) is the most influential factor of LST in the two islands while the marine environment is a unique contributor to STE of inhabited islands compared with inland cities, where the seawater around the island can reduce LST over a range of distances, and the influence of elevation on LST is mostly indirect. These results provide a scientific basis and case support for understanding the STE situation of inhabited islands with different urbanization levels.

Keywords: inhabited island; surface thermal environment; thermal pattern; marine environment; urbanization



Citation: Zhang, J.; Lin, T.; Sun, C.; Lin, M.; Zhan, Y.; Chen, Y.; Ye, H.; Yao, X.; Huang, Y.; Zhang, G.; et al. Long-Term Spatiotemporal Characteristics and Impact Factors of Land Surface Temperature of Inhabited Islands with Different Urbanization Levels. *Remote Sens.* **2022**, *14*, 4997. <https://doi.org/10.3390/rs14194997>

Academic Editor: Lunche Wang

Received: 13 September 2022

Accepted: 3 October 2022

Published: 8 October 2022

Publisher's Note: MDPI stays neutral with regard to jurisdictional claims in published maps and institutional affiliations.



Copyright: © 2022 by the authors. Licensee MDPI, Basel, Switzerland. This article is an open access article distributed under the terms and conditions of the Creative Commons Attribution (CC BY) license (<https://creativecommons.org/licenses/by/4.0/>).

1. Introduction

Given the long-term warming trend, the observed global mean surface temperature between 2006 and 2015 was 0.87 °C higher than the average over the 1850–1900 period, and global warming is likely to reach 1.5 °C between 2030 and 2052 [1]. This means greater human heat hazards since the global population could grow to around 9.7 billion by 2050 [2], with 68 percent of those projected to be urban [3]. The health of residents has been significantly affected by the quality of the thermal environment.

The thermal environment is a heat-related physical environment that can affect human perception of warmth/cold, population health, and the survival and development of residents [4], including the surface thermal environment (STE) characterized by land surface temperature (LST) and the regional canopy or boundary layer thermal environment

represented by atmospheric temperature [5]. Among them, STE is the most closely related to the life of regional residents and thus the livability of residential areas, as LST deeply affects human comfort and health by affecting the energy exchanges [6] and modulating the near-surface air temperature [7], which have been explored by many heat-related health risk studies [8–12]. The deterioration of the thermal environment has led to a diversity of direct or indirect consequences on human society, the most typical of which is the urban heat island (UHI), a phenomenon of urban temperatures being significantly higher than those in surrounding non-urban areas. This increases energy consumption for cooling [13] and leads to some environmental problems such as more frequent urban heat waves and intensification of air and water pollution, and a series of social problems such as increased morbidity and mortality of residents [14,15]. As a result, the quantitative evaluations of thermal environmental changes in residential areas have been major concerns of many urban ecology studies.

Urbanization, a vital factor affecting the spatiotemporal dynamic characteristics of STE [14], is unequal worldwide, with the largest expansion of built-up area mainly distributed in the United States and developing and emerging countries (such as China) and the largest growth of the urban population mainly concentrated in Asia and Africa [16]. In particular, the centers of gravity related to urbanization and the global population are moving to the southeastern region motivated by the expansion of China from 1960 to 2016 [17]. The global urban area expanded by 80% and the urban population increased by 52% from 1985 to 2015 [18], which has largely promoted both the demand and progress of the research on the urban thermal environment. Since Howard (1833) first proposed UHI as a result of urbanization [19] and Rao (1972) first observed surface UHIs with satellite sensors [20], there has been a proliferation of studies on urban thermal environments and urban heat islands, especially after 2005 [13]. The main research contents of existing studies can be summarized into two aspects: inwardly, the characteristics and formation mechanism of STE or UHI, including quantification and evaluation of the status of the thermal environment or the intensity of the UHI effect and identification of their influencing factors [21], such as the landscape composition and configuration [22] and artificial waste heat [14]; and outwardly, analysis of the social and environmental hazards caused by the deterioration of STE or the intensification of UHI effects, such as urban pollution [23] and the health problems of residents exposed to high temperatures [11,12]. In terms of research objects, although the range of studies covers city-specific landscapes at the micro level, such as functional zones [24] or specific land types [5], and specific cities [22,25] or urban agglomeration [26] at the macro level, relevant research has always focused on cities.

Thermal environment studies are aimed at regional residents to provide a more comfortable and livable living environment, thus adequate and abundant case studies performed in city areas have helped to understand the spatiotemporal variations of the UHI intensity in different cities [27]. Comparatively, although there are many island cities and countries around the world (such as Java, British Isles, Salsette Island, etc.), little attention has been paid to the thermal variability of inhabited islands, which are also important human habitats. On the land side of the global coastline, more than half of the world's population lives in coastal areas within about 60 km of the coast [28], and as a vital component of marine and coastal zone ecosystems, islands are significant sites and special regional units for human productive activities with unique geographical and climatic conditions. Compared with inland cities, inhabited islands and island cities are natural closed systems surrounded by seawater with distinct boundaries [29], and this particular geographical environment enables them to avoid the interference of the thermal effect from adjacent land, providing an ideal independent area for the study of thermal environmental characteristics of residential areas. It is also more representative to perform contributor analysis of STE on inhabited islands due to the sensitive response of the island ecosystem to various natural and anthropogenic factors [30]. However, most current environmental studies on islands have focused on species richness surveys [31], island ecosystem health assessments [30], and various resource and environmental effects of

human economic activities (such as tourism) [32,33]. Accordingly, it is necessary but rare to carry out thermal environment investigations on inhabited islands. Moreover, due to the lack of relevant research cases and the poor spatial synchronization owing to the instantaneous measurement of LST captured by remote sensing satellites, the comparison of STE and the UHI intensity of inhabited islands at different urbanization levels is not fully understood.

The main objective of this study was to investigate the significant differences in the characteristics and impact factors of STE in two inhabited islands with different urbanization levels under the same climate conditions and similar area size, and whether there any similarities and differences in the impact factors of STE of inhabited islands compared with previous inland cities. Two inhabited islands located in the same satellite image but at different stages of urbanization development were selected for comparative analysis from the spatial and temporal dimensions by the GIS and RS methods, and the results supplement empirical cases to the thermal environment investigation of the islands, providing the scientific basis for the urbanization development planning of the islands for the relevant decision-makers.

2. Materials and Methods

2.1. Study Area and Data Source

The study area covers the highly and rapidly urbanized Xiamen Island (main island) and the lowly and slowly urbanized Kinmen Island, both of which are located in the southern waters of China within a typical subtropical maritime monsoon climate with warm and humid conditions throughout the year (Figure 1a,b). Among them, Xiamen Island is part of Xiamen City, Fujian Province, with an “O” shape and a main island area of approximately 143.14 km², while Kinmen Island is subordinate to Quanzhou City, Fujian Province, with an “H” shape and a total island area of about 136.45 km². Despite the similar area scale and the close position, there are significant differences in both the speed and degree of urbanization between the two islands and the population. From 2000 to 2020, the GDP of Xiamen Island grew rapidly from 3.82 to 344.88 billion yuan, allowing Xiamen Island to reach an urbanization rate of 100% as early as 2010 [34], and its population had increased to 2.11 million by 2020. Comparatively, Kinmen County, whose relatively stable population was only 6.72×10^{-2} million in 2020, only had a GDP of about 22.10 billion yuan in 2020 [35]. In addition, the significant differences in the spatial extent of their urban area can also be seen in the images shown in Figure 1c–e. In short, the same climate and remote sensing imaging condition with a similar area size but the evident differences in the island shape, urbanization level, and population magnitude between Xiamen Island and Kinmen Island, and the spatial independence of each other due to the marine environment make it an ideal area for the comparative study of STE of inhabited islands.

Cloud-free Landsat-5 TM (2000/2003/2006/2010) and Landsat-8 OLI/TIRS (2014/2017/2020) images (Table A1), and 30 m spatial resolution DEM data, Shuttle Radar Topography Mission 1 (SRTM1), were acquired from the United States Geological Survey (USGS) while the vector boundary data of islands were modified from Resources and Environmental Science and Data Center of Chinese Academy of Sciences. The latest DEM data (NASADEM) was obtained from the website of NASA EarthData, and the data of near-surface mean air temperature used for LST retrieval were collected from the official yearbooks.

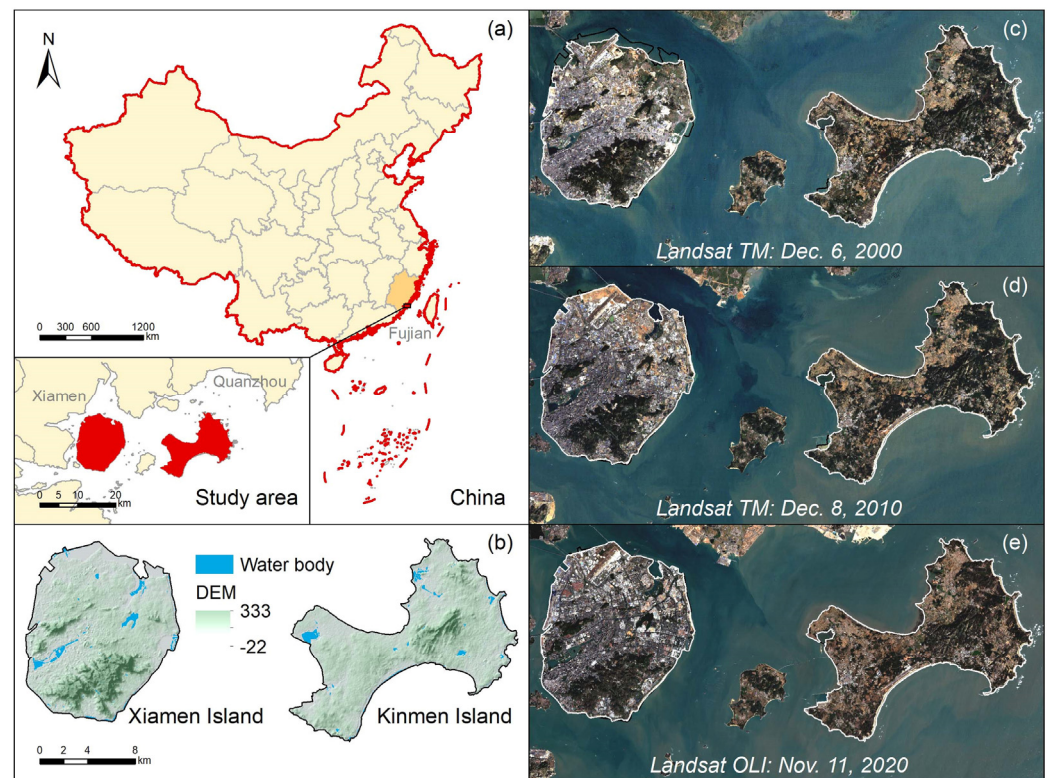


Figure 1. Geographical location of the study area and the presentation of geographical data. (a) Location of the study area in China; (b) Comparison of topography features between Xiamen Island and Kinmen Island based on DEM; (c–e) Decadal spatial distribution of the land surface of the study area.

2.2. Retrieving LST with Mono-Window Algorithm

In consideration of the characteristic of Landsat thermal data, a mono-window algorithm proposed by Qin et al. [36] was used to retrieve LST, which directly includes the atmospheric influence in the calculation equation to avoid atmospheric simulation errors compared with the radiative transfer equation method [36,37], and obtains a slightly higher LST calculation accuracy than that of the single channel algorithm in some comparative studies [37–39]. Although proposed for Landsat TM6 data initially, it also performs well for Landsat TIRS data [40]. The specific retrieval method of the land surface temperature T_s is shown in Equation (1), whose meanings of variables are detailed in Table 1:

$$T_{\lambda s} = [a_{\lambda}(1 - C_{\lambda} - D_{\lambda}) + (b_{\lambda}(1 - C_{\lambda} - D_{\lambda}) + C_{\lambda} + D_{\lambda})T_{\lambda t} - D_{\lambda}T_a]/C_{\lambda} \quad (1)$$

To eliminate the inconsistency of LST and thus improve the comparability in the time dimension to obtain more objective rules, the mean-standard deviation method [41] was used to divide LST into a hot zone, normal zone, and cold zone to characterize the thermal environment in more detail (Table 2). On this basis, the heat amplitude was defined as the ratio of the area percentage of the hot zone to that of the other zones in this study to emphasize the gap in the spatial extent of LST disparity while the heat intensity was defined as the ratio of the area percentage of the high LST zone to that of other zones, focusing more on the attribute gap of LST disparity.

Table 1. Variables and description in the formula of the mono-window algorithm [36–40].

Variables	Meaning and Expression/Value
a_λ, b_λ	Constant coefficient $a_6 = -67.355351, b_6 = 0.458606$ (0–70 °C) $a_{10} = -62.7182, b_{10} = 0.4339$ (0–50 °C)
$T_{\lambda t}$	Effective at-satellite brightness temperature (K) calculated by the DN value for the quantized and calibrated standard product pixel of TM6/TIR10 image (Q_{DN}) $T_{6t} = 1260.56 / \ln[1 + 607.76 / (1.2378 + 0.055158Q_{DN})]$ $T_{10t} = 1321.08 / \ln[1 + 774.89 / (0.1 + 0.0003342Q_{DN})]$
T_a	Effective mean atmospheric temperature obtaining by the near surface air temperature T_0 $T_a = 19.2704 + 0.91118T_0$ (for mid-latitude winter)
C_λ, D_λ	Internal parameter $C_\lambda = \varepsilon_\lambda * \tau; D_\lambda = (1 - \tau) * (1 + (1 - \varepsilon_\lambda) * \tau)$
τ	Atmospheric transmittance obtained from https://atmcorr.gsfc.nasa.gov/ (accessed on 17 February 2021)
ε_λ	Ground emissivity consisting of the emissivity of representative terrestrial materials (water, soil, impervious surface, and vegetation) for band λ $\varepsilon_{water} = \varepsilon_{\lambda w}; \varepsilon_{surface} = \varepsilon_{\lambda v}C_V + \varepsilon_{\lambda s}(1 - C_V); \varepsilon_{building} = \varepsilon_{\lambda v}C_V + \varepsilon_{\lambda i}(1 - C_V)$ $(\varepsilon_{6w} = 0.995, \varepsilon_{6s} = 0.972, \varepsilon_{6i} = 0.970, \varepsilon_{6v} = 0.986; \varepsilon_{10w} = 0.991, \varepsilon_{10s} = 0.966, \varepsilon_{10i} = 0.962, \varepsilon_{10v} = 0.973)$
C_V	Vegetation coverage $C_V = [(NDVI - NDVI_S) / (NDVI_V - NDVI_S)]^2$ $NDVI_S = 0.2; NDVI_V = 0.5$
$NDVI$	The normalized differential vegetation index obtaining by near infrared band (ρ_{NIR}) and infrared (ρ_R) $NDVI = (\rho_{NIR} - \rho_R) / (\rho_{NIR} + \rho_R)$

Table 2. Statistic basis of LST zoning.

Primary Zoning	Detailed Zoning	Conditions *
Hot zone	High LST zone (HTZ)	$T_s > \mu + std$
	Sub high LST zone (SHTZ)	$\mu + 0.5std < T_s \leq \mu + std$
Normal zone	Medium LST zone (MTZ)	$\mu - 0.5std \leq T_s \leq \mu + 0.5std$
Cold zone	Sub low LST zone (SLTZ)	$\mu - std \leq T_s < \mu - 0.5std$
	Low LST zone (LTZ)	$T_s < \mu - std$

* μ : mean LST; std : standard deviation of LST.

2.3. Identifying Land Cover Types with SVM Classification

According to the actual situation of islands and research demands, land cover types were defined as the following four categories: greenland (the area covered with vegetation, including forestland, grassland, and cultivated land with vegetation); impervious surface (the area of artificial hard surface, including settlements, traffic land, and industrial land); bare land (natural bare land without vegetation cover, including unused land, fallow arable land, and sandy beach); and water body (including lakes, reservoirs, and rivers).

Given the limited size of the study area, a support vector machine (SVM) in the machine learning classifier was used to identify land cover types due to its advantage of achieving high classification accuracy with small training data sets [42]. Through further post-classification, the final land cover classification results that met the accuracy requirements and were feasible for subsequent analysis with a Kappa coefficient exceeding 0.85 and overall accuracy exceeding 90% were obtained after being verified by the region of interest (ROI) samples determined from the original remote sensing images through visual interpretation.

2.4. Measuring the Spatial Heterogeneity of LST

Moran's I [43] and Getis-Ord G_i^* [44] were used to measure the spatial heterogeneity of LST in this work, of which the former is an overall statistical description of the spatial

autocorrelation of LST based on feature locations and attributes of the elements, and the latter gives further statistical identification and clear visualization of the significant hot spots and cold spots of LST. Their basic formulas are shown in Equations (2) and (3), respectively, and more detailed information can be found in the literature [43,44]:

$$I = \left[n \sum_{i=1}^n \sum_{j=1}^n w_{ij} (x_i - \bar{x})(x_j - \bar{x}) \right] / \left[\sum_{i=1}^n \sum_{j=1}^n w_{ij} \sum_{i=1}^n (x_i - \bar{x})^2 \right] \tag{2}$$

$$G_i^* = \left[\sum_{j=1}^n w_{ij} x_j - \left(\sum_{j=1}^n x_j \sum_{j=1}^n w_{ij} / n \right) \right] / \left\{ \sqrt{ \left[n \sum_{j=1}^n x_j^2 - \left(\sum_{j=1}^n x_j \right)^2 \right] \left[n \sum_{j=1}^n w_{ij}^2 - \left(\sum_{j=1}^n w_{ij} \right)^2 \right] / [n^2(n-1)] } \right\} \tag{3}$$

where x_i is the attribute for feature i , \bar{x} is the mean of the corresponding attribute, w_{ij} is the spatial weight between feature i and j , and n is the total number of features.

2.5. Analyzing the Thermal Landscape Pattern with Geographic Distribution and Landscape Metrics

The geographic center of the high LST zone of the two inhabited islands was measured by the mean center (Equation (4)), and the directional distribution ellipse (Equation (5)) was used to show the spatial characteristics of the dispersion and direction trend of the high LST zone [45]:

$$MC = \begin{cases} \bar{x} = \frac{1}{n} \sum_{i=1}^n x_i \\ \bar{y} = \frac{1}{n} \sum_{i=1}^n y_i \end{cases} \tag{4}$$

$$C = \frac{1}{n} \begin{bmatrix} \sum_{i=1}^n (x_i - \bar{x})^2 & \sum_{i=1}^n (x_i - \bar{x})(y_i - \bar{y}) \\ \sum_{i=1}^n (x_i - \bar{x})(y_i - \bar{y}) & \sum_{i=1}^n (y_i - \bar{y})^2 \end{bmatrix} \tag{5}$$

where (\bar{x}, \bar{y}) and (x_i, y_i) are the coordinates of the mean center and element i , respectively, and n is the total number of elements.

Based on landscape ecology methods, the landscape metrics [46] were used to assess the thermal landscape pattern by exploring the fragmentation, aggregation, and shape complexity of the high LST zone patch (Figure A1), and produce grid layers of diverse land coverage rates (Figure A2). Specifically, to enhance the spatial correspondence between LST and land cover type in the contributor analysis, a 210 × 210 m window (Figure A3) was used to move pixel by pixel on the land cover type grid, during which the calculated value of the landscape percentage index (PLAND) of the whole window was assigned to the pixel in the center of the window and thus the spatially continuous coverage rate images of each land class were obtained. The specific expression and meaning of each landscape metric are shown in Table 3.

Table 3. The formula and significance of landscape metrics.

Characteristics	Metrics and Expression *	Meaning
Fragmentation	$PD = (n_i/A) \times 10000 \times 100$	The larger the patch density ($PD \geq 0$), the more broken the thermal landscape.
Aggregation	$AI = 100 \times g_{ii}/maxg_{ii}$	The larger the aggregation index ($0 \leq AI \leq 1$), the more concentrated the thermal landscape is in space.

Table 3. Cont.

Characteristics	Metrics and Expression *	Meaning
Shape complexity	$FRAC_MN = 2 \ln(0.25p_{ij}) / \ln a_{ij}$	The larger the fractal dimension index ($0 \leq FRAC_MN \leq 1$), the more complex the path shape of the thermal landscape.
Area proportion	$PLAND_i = 100 \times \sum_{j=1}^n a_{ij} / A$	The larger the percentage of landscape ($0 \leq PLAND \leq 100$), the larger the area proportion of the patch type i . In this study, a moving window with a pixel size of 210 by 210 m was used to calculate $PLAND_i$ of each pixel position in the research area to generate a continuous raster layer of the land cover rate in space.

* n_i : number of patches in the landscape of path type i ; A : total landscape area (m^2); p_{ij} : perimeter of the patch ij ; a_{ij} : area of patch ij (m^2); g_{ij} : number of like adjacencies between pixels of patch type i based on the single-count method, whose maximum was defined as $maxg_{ij}$.

2.6. Exploring the Impact Factors of LST with Spearman's Rho

Spearman's rank correlation coefficient [47], also called Spearman's rho, is a non-parametric test method used to measure the linear or nonlinear correlation between two variables, which is widely applicable because of the no normal distribution requirement and insensitivity to outliers [48]. Considering the interference of outliers with the results and the spatially continuous variables that all meet the requirements of a normal distribution, Spearman's rho was used to explore the impact factors of LST (Equation (6)):

$$r_s = 1 - \left[6 \sum_{i=1}^n d_i^2 / n(n^2 - 1) \right] \quad (6)$$

where r_s ($-1 \leq r_s \leq 1$) is the Spearman's rho, d_i is the ranking deviation of corresponding observes values, and n is the number of observed values.

3. Results

3.1. Spatiotemporal Characteristics of LST in the Two Inhabited Island

3.1.1. Retrieve Results and Spatial Heterogeneity of LST

In terms of time series, taking 2010 as the turning point, the mean LST of the two inhabited islands showed obvious fluctuations in the first 10 years of the study period but continued to rise in the last 10 years, which as a result increased by 2.01 °C in Xiamen Island and 3.29 °C in Kinmen Island, respectively (Figure 2). From the perspective of spatial comparison, the mean LST was slightly higher on Xiamen Island from 2000 to 2010 but on Kinmen Island after 2010.

According to the positive Moran's I, which ranged from 0.95 to 0.99 at the 0.01 significance level, significant spatial cluster patterns of LST existed in both Xiamen Island and Kinmen Island in all periods, whose geographical spatial distribution was characterized by the cold/hot spot area as shown in Figure 2. From 2000 to 2020, the area proportion of hot spot regions (with a confidence level of 0.9 or above) of LST increased in both islands, and 5.06% and 5.78% of the spatiotemporal stable hot spot regions were retrieved in Xiamen Island and Kinmen Island, respectively, which may provide supplementary information for the identification of the small regional-scale UHI.

3.1.2. Spatiotemporal Characteristics of the Thermal Effect

Evident differences in the spatiotemporal characteristics of the LST zoning based on the retrieved results of LST between the two islands are revealed in Figure 3a. Specifically, the area proportion of the high LST zone wavelike increased by 10.09% during the study period whereas that of the hot zone wavelike decreased by 2.57% due to the reduced sub-high LST zone in Xiamen Island while the opposite trend was correspondingly found in the low LST zone and cold zone, suggesting enhancement of the heat intensity due to the more and more extreme LST despite the mitigating heat amplitude. In contrast, intensified

heat amplitude and reduced heat intensity were found in Kinmen Island according to the increase in the area proportion of the hot zone (12.00%) and the decrease in that of the high LST zone (−5.42%). As a result, a weaker mean heat intensity but stronger heat amplitude were found on Xiamen Island (Figure 3b,c).

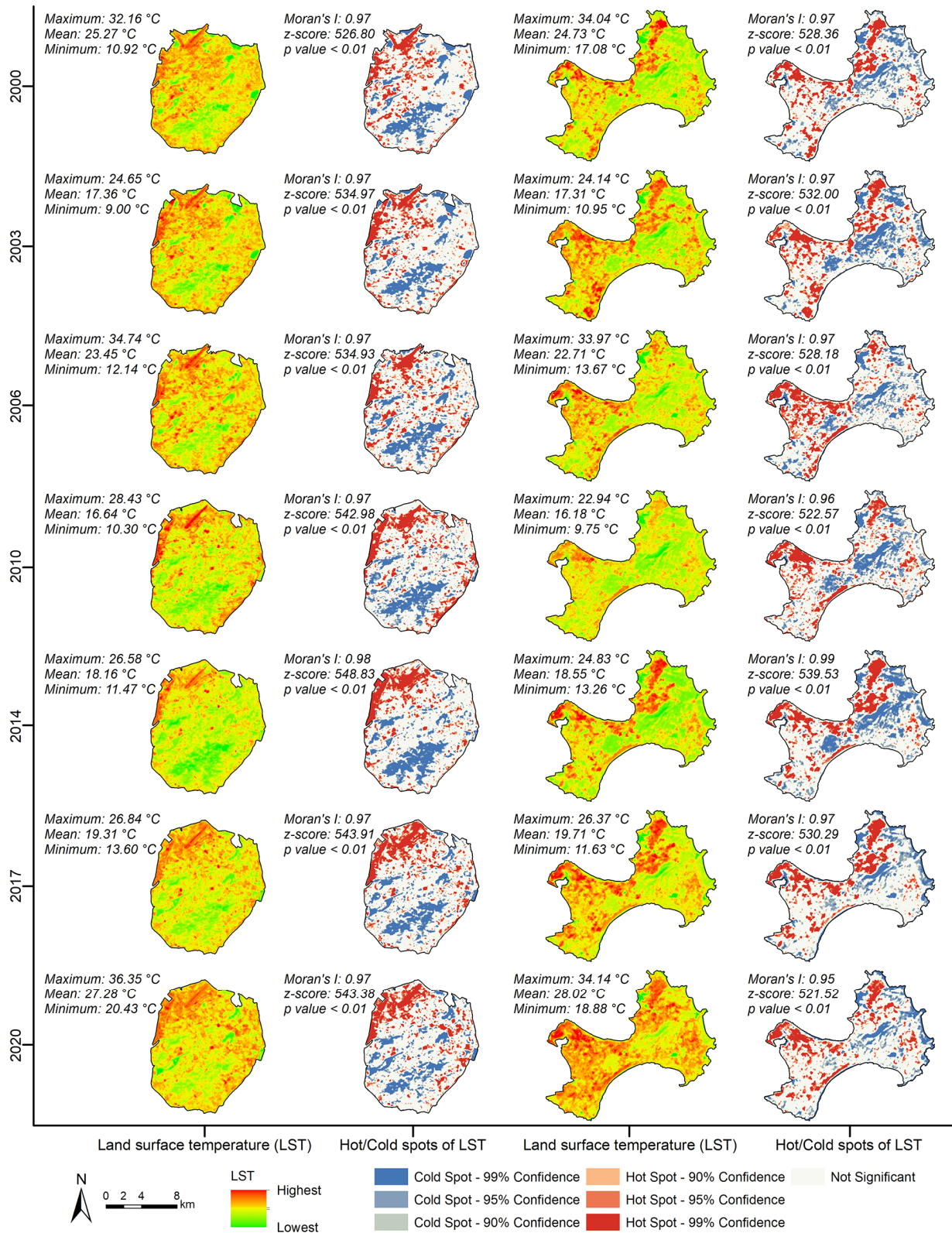


Figure 2. LST and its spatial heterogeneity in the two inhabited islands from 2000 to 2020.

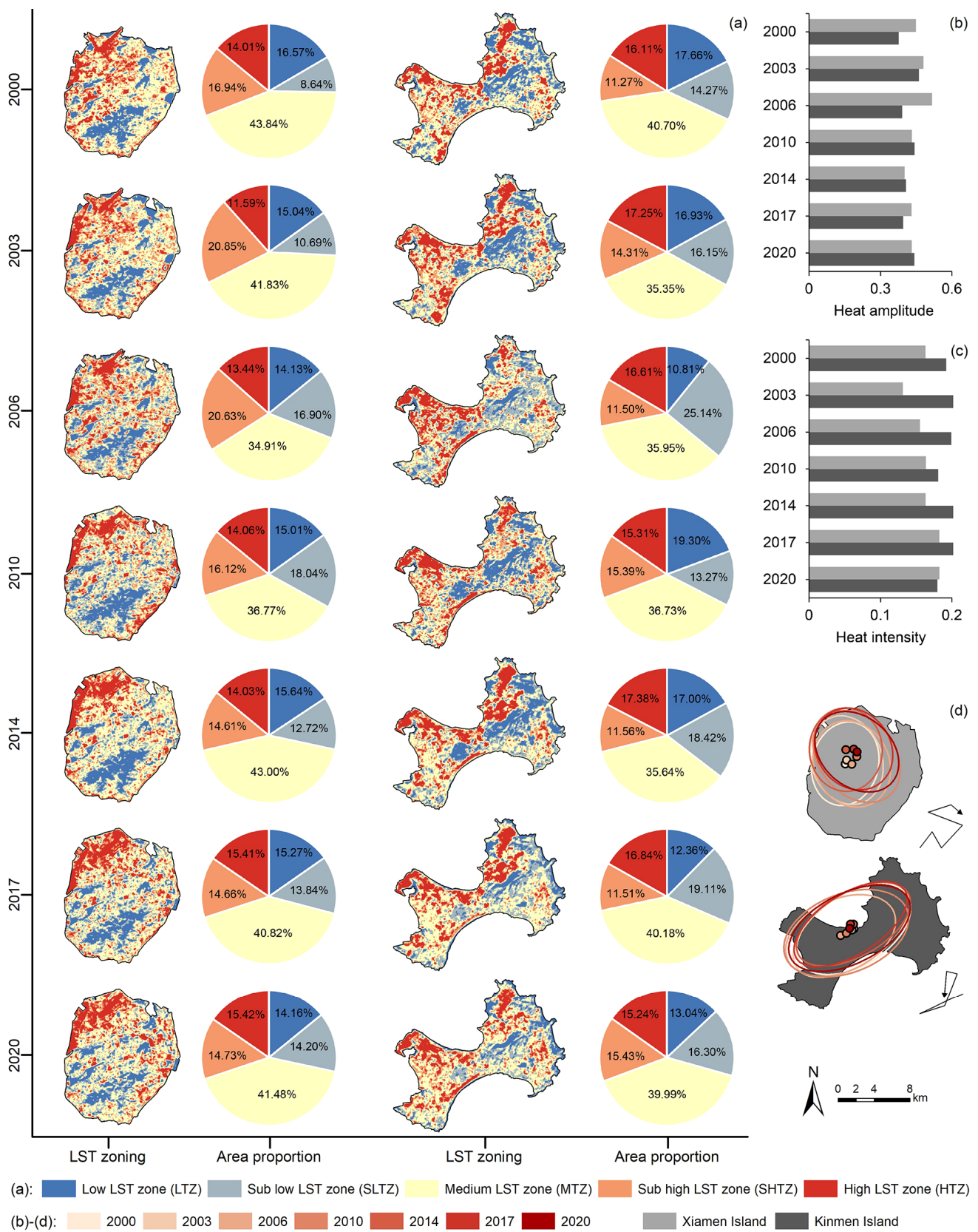


Figure 3. The spatiotemporal change and comparison of STE between Xiamen Island and Kinmen Island from 2000 to 2020. (a) The distribution and area proportion of LST zoning; (b) Heat amplitude change; (c) Heat intensity change; (d) Geographical distribution (mean center and directional distribution ellipse) change in HTZ.

Different from the relatively spatiotemporal stable distribution of the hot zone in Kinmen Island, which was mainly concentrated in the west and north of the island, the primary spatial distribution of the hot zone in Xiamen Island dynamically shifted from the west and north of the island to the northwest and east coast of the island from 2000 to 2020. Distinct differences in the geographical distribution characteristic of a high LST zone between the two islands are shown in Figure 3d. The mean center of the high LST zone in Xiamen Island was stably located in the northwest of the island and migrated as “S” over time while the direction distribution ellipse of the high LST zone changed from the “northeast to southwest” direction with smaller eccentricity to the “northwest to southeast” direction with larger eccentricity. At the same time, the mean center of the high LST zone in Kinmen Island was stable near the northern bay area and moved anticlockwise, with the direction distribution ellipse keeping the direction of “northeast to southwest” with increasing eccentricity.

On this basis, there were opposite temporal trends of landscape pattern characteristics of the thermal patches between the two islands according to the landscape metrics (Table 4), where increasingly contiguous and gathered but decreasingly shape-complex thermal patches were revealed in Xiamen Island while increasingly fragmented and scattered and shape-complex thermal patches in Kinmen Island. On the whole, the thermal patches of Xiamen Island were more fragmented, discrete, and shape-simple than that of Kinmen Island on average over the study period.

Table 4. Fragmentation, aggregation, and shape complexity of the thermal landscape (HTZ) between Xiamen Island and Kinmen Island in different periods.

Year	Xiamen Island			Kinmen Island		
	PD	AI	FRAC_MN	PD	AI	FRAC_MN
2000	2.2649	85.9005	1.0573	1.2679	90.4604	1.0541
2003	1.5422	87.6945	1.0521	1.0010	90.8477	1.0624
2006	2.0362	87.7630	1.0483	2.0019	87.6046	1.0537
2010	1.6256	88.0171	1.0564	3.9298	84.0374	1.0513
2014	1.5974	89.3791	1.0515	1.0561	92.1826	1.0539
2017	1.9141	88.4897	1.0522	1.0044	91.8410	1.0555
2020	1.6607	88.9447	1.0509	1.3958	89.7056	1.0585
Average	1.8059	88.0269	1.0527	1.6653	89.5256	1.0556

3.2. Impact Factors of LST in the Inhabited Islands

3.2.1. Land Cover Types and Their Effects on LST

The spatial distribution of the land cover type of the study area shown in Figure 4a denotes that more than one-third of the highly urbanized Xiamen Island was covered by an impervious surface, which continued to spread to the north and east of the island via the occupation of other land types and as a result of the increased area proportion from 42.04% to 49.43% during the study period (Figure 4b). Numerous stable green landscapes, the second major and increasing land cover type of Xiamen Island with an area proportion of 39.03% in 2020, were distributed mostly in the southern and western mountains. In addition, although the total area of the entire island increased by 7.88 km² owing to the extensive sea reclamation in the north of the island from 2000 to 2010, the area proportion of inland water body decreased from 5.60% in 2000 to 2.72% in 2010, and 2.79% in 2020. Different from Xiamen Island, Kinmen Island maintained a stable land cover pattern that was dominated by greenland (58.83% on average), and its low impervious surface was mainly clustered along the bay coast of the eastern island and on the west side of the southeastern island lake.

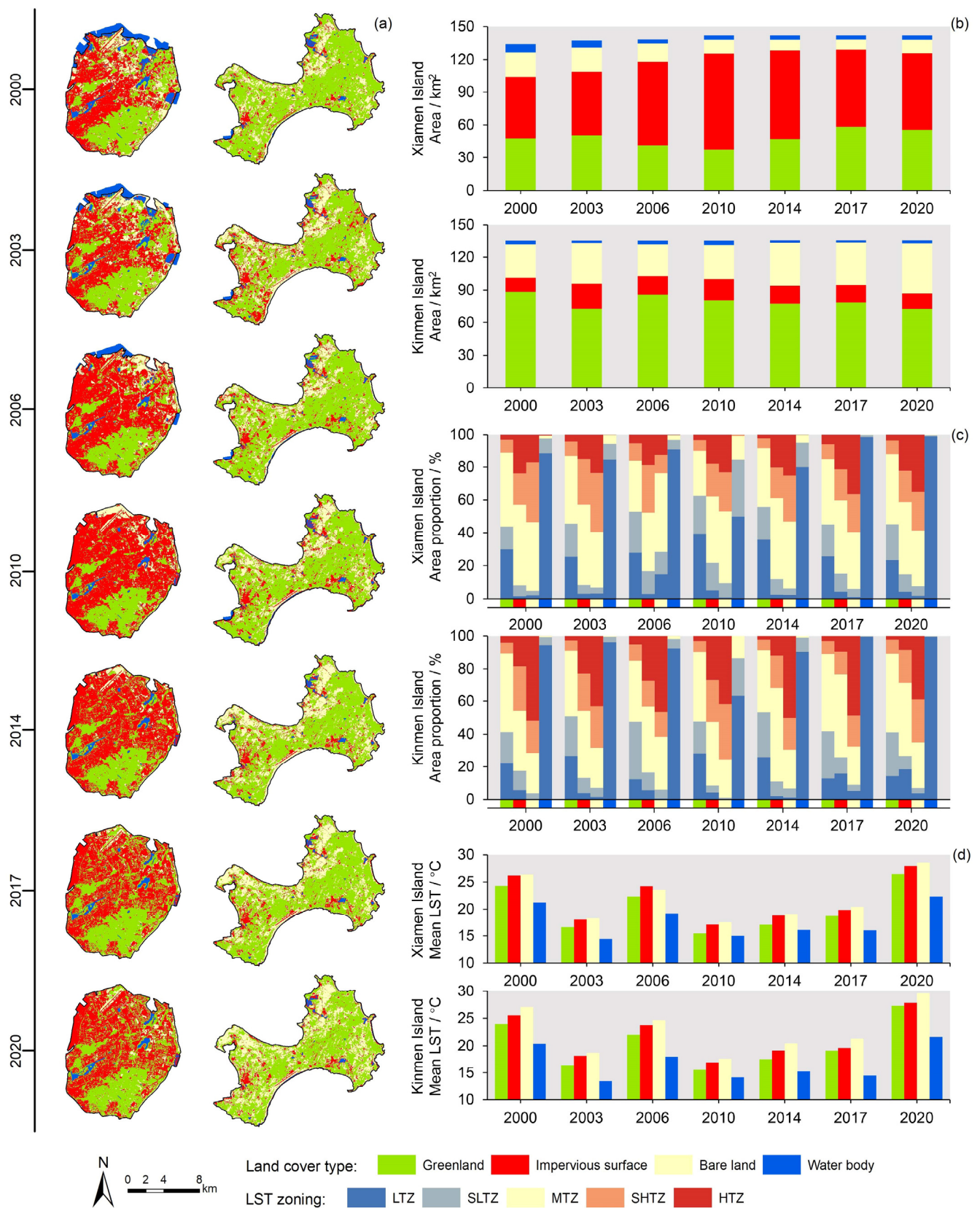


Figure 4. Spatiotemporal change in land cover and their effects on LST in the two islands from 2000 to 2020. (a) Identification results of land cover; (b) Change in the area of land cover types; (c) Area proportion of LST zones over different land cover types; (d) Comparison of mean LST over different land cover types.

A consistent spatial correspondence of the LST zoning and land use pattern was found in the two islands when comparing Figures 3a and 4a. Except for MTZ, the distribution area of greenland and water body was the largest in the cold zone (LTZ or SLTZ) while that of bare land and impervious surface was the largest in the hot zone (Figure 4c), indicating that for both Xiamen Island and Kinmen Island, bare land and impervious surface can be proposed as warming land patches while greenland and water body are cooling land patches. Among them, bare land exacerbated LST more than impervious surface, and water body mitigated LST better than greenland according to the statistical results of the mean LST by land category shown in Figure 4d.

In consideration of the one-sidedness of the classification statistical results, which cannot fully determine the thermal effect of each land cover type from the perspective of continuous spatial correspondence, we performed a comprehensive statistical analysis on the relationship between the spatial continuous layers of cooling/warming land coverage (measured by PLAND in Figure A2) and LST, and the results are shown in Figure 5a.

3.2.2. Comprehensive Analysis of Multiple Factors of LST

Figure 5a–c shows the variation trend of LST with PLAND of cooling land, coastal distance, and elevation, respectively. The significant negative correlation relationship between LST and PLAND of cooling land was qualitatively revealed by the density scatter plot and quantitatively revealed by Spearman's rho (r_s). For all spatial locations (raster pixels) across the study area, there was a monotonically declining trend of the mean LST with the increase in PLAND of cooling land, providing complementary spatial and attribute verification information for the classification of cooling/warming land patches.

As shown in Figure 4a, the coastline of Xiamen Island changed dramatically from 2000 to 2010 because of the significant increase in the island area caused by coastal reclamation while the coastline of Kinmen Island remained relatively stable during the study period. On the whole, according to Figure 5b, there seems to be a significant slight negative correlation between LST and coastal distance of the two islands, except that of Kinmen Island in 2017 and 2020.

An evident negative relationship also existed between LST and elevation on the space-time dimension as shown in Figure 5c, indicating the possible effectiveness of an elevation increase in mitigating LST. Additionally, it is interesting to note that LST decreased rapidly with the increase in elevation in the interval of 0–100 m, but the rate of decrease slowed down obviously when the elevation reached above 100 m.

In consideration of a single contributor for Xiamen Island, PLAND of cooling land, elevation, and coastal distance were significantly negatively correlated with LST (Figure 5d). Among them, PLAND of cooling land had the greatest influence on LST, followed by elevation and coastal distance. The results of Kinmen Island were similar except for the positive correlation between coastal distance and LST in 2017 ($r_s = 0.10$) and 2020 ($r_s = 0.06$). However, significant correlations were also found among the three impact factors. Therefore, to eliminate the interference of the significant correlation between the three contributors on the influencing mechanism analysis of STE, the partial correlation coefficients via Spearman's rho (pr_s) [49] between LST and the three impact factors were calculated (Table 5).

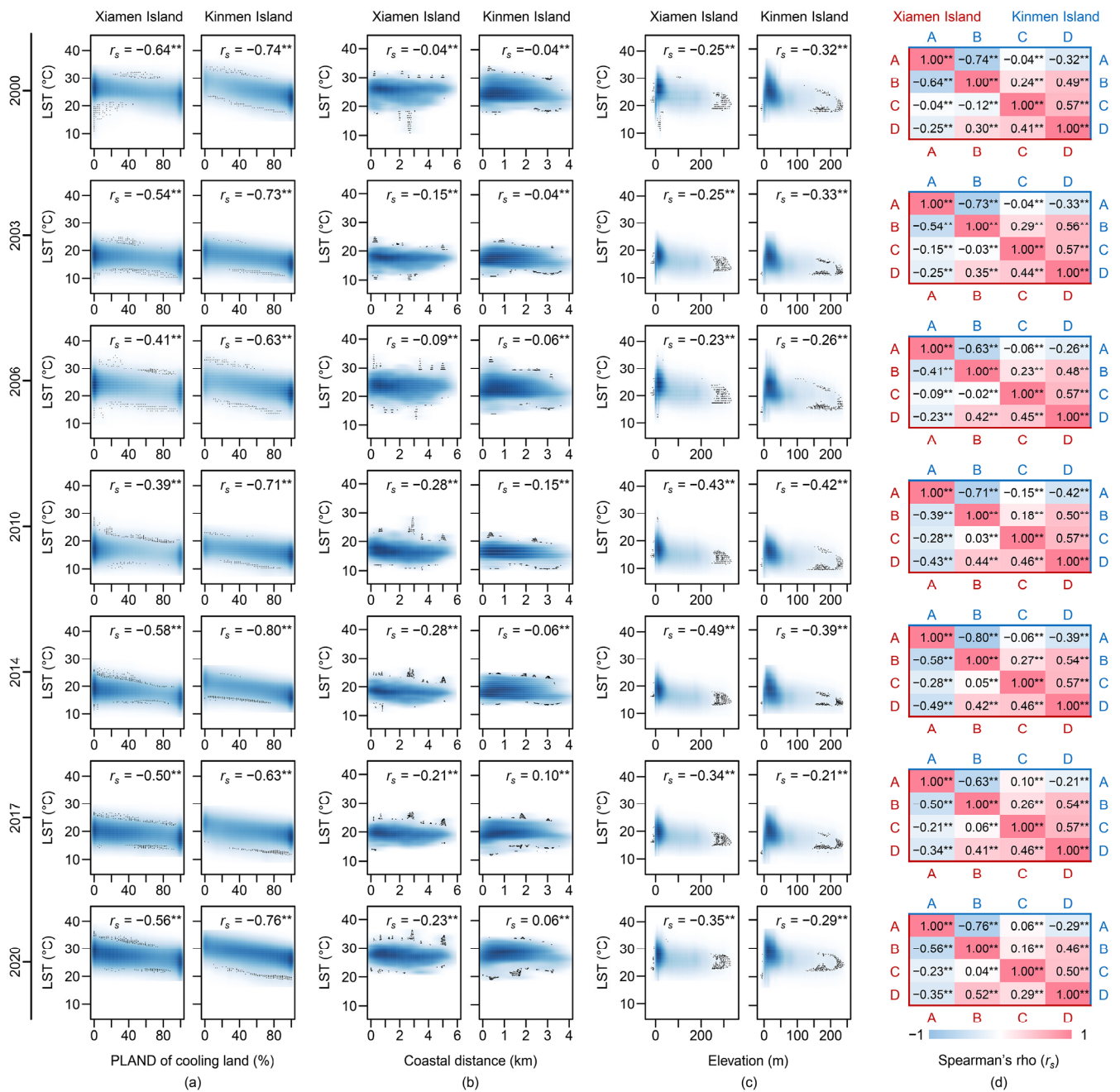


Figure 5. Correlation between LST and its impact factors in the two islands from 2000 to 2020. (a) The effect of PLAND of cooling land on LST (the opposite trend for PLAND of warming land); (b) The effect of coastal distance on LST; (c) The effect of elevation on LST; (d) Thermal map of Spearman’s rho among variables (A: LST; B: PLAND of cooling land; C: coastal distance; D: elevation). ** at the 1% significance level.

There was still a strong and significant negative correlation between LST and PLAND of cooling land when given other variables ($pr_s \leq -0.27$ in Xiamen Island and $pr_s \leq -0.60$ in Kinmen Island), demonstrating that land cover type is the most important factor affecting LST, and its influence on LST is direct to a large extent. However, the absolute value of the partial correlation coefficient between elevation and LST decreased significantly both on Xiamen Island and Kinmen Island when given two other variables. Based on the relationship between elevation and the other two variables in Figure 5d, it can be seen that elevation mainly affected LST indirectly by changing the landscape composition, and its direct influence was limited. In addition, the positive and negative properties were

unstable. Of particular concern, there was a significant positive correlation between coastal distance and LST in Kinmen Island when given other variables, i.e., the closer to the coast, the lower the LST, which means that seawater has a positive effect on reducing island LST.

Table 5. Partial correlation coefficient with Spearman's rho (ρ_s) between LST and other variables.

Year	Xiamen Island			Kinmen Island		
	PLAND of Cooling Land	Coastal Distance	Elevation	PLAND of Cooling Land	Coastal Distance	Elevation
2000	−0.62 **	−0.14 **	0.00	−0.70 **	0.20 **	−0.05 **
2003	−0.52 **	−0.18 **	0.02 **	−0.71 **	0.22 **	0.02 **
2006	−0.36 **	−0.08 **	−0.02 **	−0.60 **	0.10 **	0.00
2010	−0.27 **	−0.16 **	−0.21 **	−0.63 **	0.03 **	−0.11 **
2014	−0.49 **	−0.18 **	−0.22 **	−0.77 **	0.25 **	−0.06 **
2017	−0.43 **	−0.14 **	−0.09 **	−0.64 **	0.30 **	0.02 **
2020	−0.56 **	−0.19 **	0.08 **	−0.73 **	0.28 **	0.06 **

** At the 1% significance level.

3.2.3. Further Analysis of the Effect of the Marine Environment on LST

In view of the opposite partial correlation analysis results of the two islands, we calculated the mean LST in different coastal distance regions with the basic distance unit of 30 m to further explore the influence of the marine environment on LST of these two inhabited islands. Considering the strong influence of the land cover type on LST proved above, both classified statistics according to land cover and comprehensive statistics were carried out, and the results are shown in Figure 6a.

The comprehensive analysis results (histogram in Figure 5) show that for Xiamen Island and Kinmen Island, the smaller the coastal distance, the lower the mean LST within a specific distance range, indicating that the marine environment did mitigate LST in the coastal area to a certain extent. Taking the first turning point of the broken line of the mean LST change in different distance intervals as the distance threshold of the impact of coastal seawater on LST, it can be seen that for both islands, the influence of coastal distance on the water body was unstable within the threshold, so no obvious cooling effect was found. However, the other three land cover types all showed an obvious cooling trend with the decrease in the coastal distance, especially on Kinmen Island. No stable and consistent size pattern of the threshold values of different land cover types on the time series was found. Specifically, for the other three types of land use, the threshold values were 150–330 m for greenland, 150–390 m for impervious surface, and 300–390 m for bare land in Kinmen Island; and 60–210 m for greenland, 120–210 m for impervious surface, and 90–270 m for bare land in Xiamen Island.

Moreover, corresponding to the influence of the marine environment on island LST, the obvious warming effect of the island environment on the surrounding seawater was also revealed, that is, the closer the seawater was to the coast, the higher the mean LST, which was particularly evident in the highly urbanized Xiamen Island (Figure 6b).

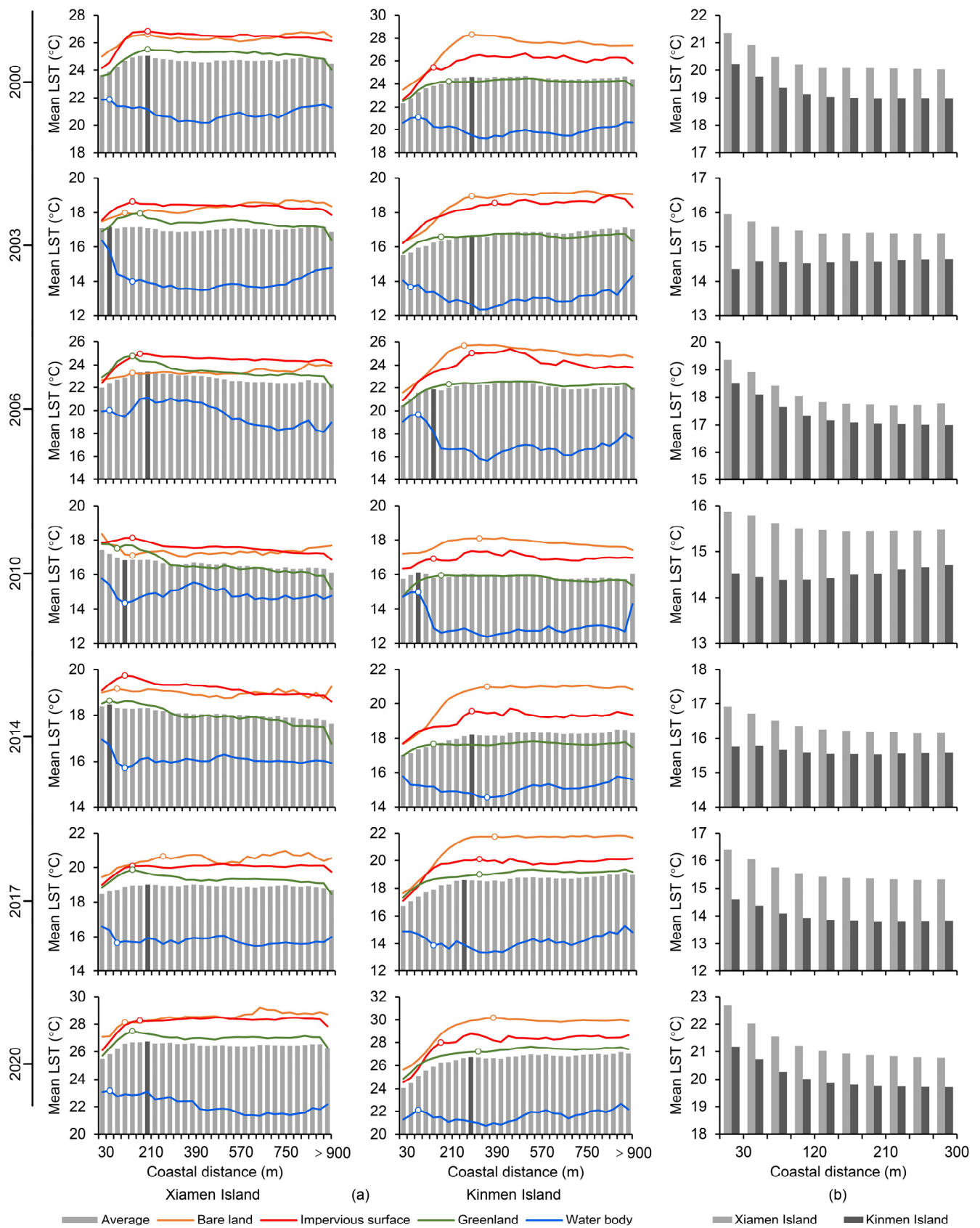


Figure 6. Variation of mean LST with coastal distance in the two islands from 2000 to 2020. (a) Mean LST of various land types at different coastal distances based on a 30 m distance resolution; (b) Comparison of mean LST of seawater at different coastal distances.

4. Discussion

4.1. Differences in STE of Inhabited Islands with Various Urbanization Levels

There are evident differences in the characteristics of STE between Xiamen Island and Kinmen Island, which have the same climatic and natural geographical conditions. In terms of temporal changes, the heat amplitude of Xiamen Island decreased, but LST became increasingly extreme and the heat intensity gradually strengthened. While the heat intensity weakened and the heat amplitude increased on Kinmen Island at the same time. In terms of spatial comparison, the heat amplitude of Xiamen Island was generally stronger than that of Kinmen Island but slighter in heat intensity, and significant differences in the degree of spatial heterogeneity and geographic distribution characteristics of HTZ existed in the two islands.

PLAND of cooling/warming land is the primary contributor to STE revealed by the results in Section 3.2. Thus, the differences in the STE characteristics between Xiamen Island and Kinmen Island can be accounted for by the diversity in their land cover types. The highly urbanized Xiamen Island has an impervious surface with an area share of over 40%, meaning that the area of warming land accounts for more than 56%. In contrast, Kinmen Island is dominated by cooling land (the area accounts for more than 55%), leading to a lesser area proportion of the hot zone and a small heat amplitude. It is important proof that the level of urbanization will cause differences in the STE characteristics of different islands.

Moreover, it is noteworthy that coastal distance, a representative of the natural contributor to STE in this study, showed a negative correlation with STE on Xiamen Island but a positive correlation on Kinmen Island as a whole, which may also be related to the urbanization level. Kinmen Island, with a low urbanization level, maintains a more primitive island ecological environment, which ensures less anthropogenic disturbance to LST, and thus the reduction in coastal distance has a significant effect on mitigating LST. While this fact is the opposite on the highly urbanized Xiamen Island. A possible reason may be that other probable impact factors of STE brought by urbanization development, such as building morphology, ventilation corridors, socio-economics, and anthropogenic heat emissions [14,26,50], were not seriously controlled for in this study. Additionally, the mean LST of the seawater around Xiamen Island was found to be higher than that around Kinmen Island (Figure 6b), which may also be the result of more frequent human activities along the coast in the high urbanization of Xiamen Island.

4.2. Comparison of the Impact Factors of LST between Island Cities and Inland Cities

Compared to inland cities, the impact factors of LST of inhabited island cities are universal, reflecting that bare land and impervious surface are typical warming land patches while water body and greenland are good cooling land patches both in inland cities [50] and islands [51]. Among them, the warming capacity of bare land is stronger than impervious surface, and the cooling capacity of water body is stronger than greenland [52].

On the other hand, the contributors of LST of inhabited island cities are typical, being embodied in the island morphology and marine environment. First, the mountainous areas of Xiamen Island are mainly concentrated in the south of the island, leaving a large area of flat terrain that is densely distributed in built-up areas. Meanwhile, the coast of Xiamen Island has also become the main distribution area of the thermal landscape with the advancement of urbanization and the increase in the population. In this case, the round cake shape of Xiamen Island makes its area-weighted mean center of the thermal landscape always located in the residential area of the island (Figure 3d). Compared with Xiamen Island, the dumbbell-shaped island shape of Kinmen Island has more opportunities to make the mean center of the thermal landscape located on the seawater outside the island rather than on the island or adjacent cities for inland cities, which reduces the influence of the high-temperature environment on the residents of the inhabited island to a certain extent. Second, the ability of seawater to mitigate the thermal effects of coastal areas has also been proved as LST of coastal areas increases away from the coastline into the land

within an obvious spatial threshold. Accordingly, the island morphology and marine environment should be fully considered to optimize STE and enhance the livability of inhabited islands as much as possible in the process of urbanization development.

4.3. Limitations and Future Works

Due to data limitations, this study only focused on STE and did not carry out joint research on the canopy or boundary layer thermal environment. Moreover, the data in this study mainly reflected STE of inhabited islands during the daytime in winter. The seasonal and diurnal differences in STE have also been demonstrated by many relevant studies in cities [26,27,50]. On the other hand, LST captured by remote sensing images is an instantaneous measure at a specific moment [6,22]. To obtain a more comprehensive understanding of the characteristics and impact factors of STE and avoid the contingency of the results, all seven useful periods spanning 20 years were selected in this study. Nevertheless, the temporal resolution was still coarse. Finer temporal resolution is beneficial to better reveal the variation characteristics and details of the surface thermal environment of islands, which was also proven in this work. The combination of multi-source data should be considered in the future to expand both the breadth and depth of research on STE of islands.

Moreover, the three impact factors involved in this study are macro scale such as geographical and landscape factors, so the lack of some urban metrics on the micro scale has brought a degree of limitation to this study. For example, the urban spatial structure, which includes the characteristics of urban streets, road widths, and heights and three-dimensional forms of buildings [53], may affect STE by changing the ventilation conditions and thus the heat exchange process of the city. Finally, only the composition of land types was regarded without considering the configuration and function of land [22,25,54], which requires more accurate and effective classification methods in the identification of urban land types in future works [55].

5. Conclusions

This study investigated the characteristics and impact factors of STE on two inhabited islands in China with different urbanization levels. The results indicate that the heat amplitude weakened but the heat intensity continued to strengthen due to the increasingly extreme LST of Xiamen Island from 2000 to 2020 while that of Kinmen Island was the opposite. Although a significant cluster pattern of LST zoning was found in both islands, different geographical distributions of HTZ were among them. The thermal landscape of Xiamen Island is more fragmented, discrete, and simple in shape, and the mean center of HTZ is always located inside Xiamen Island but sometimes in the seawater of the northern bay area of Kinmen Island, resulting from the shape of the island. The land cover type is the primary contributor of STE in the two islands, followed by the coastal distance. Despite the correlation between coastal distance and LST being negative in Xiamen Island but positive in Kinmen Island as a whole, the marine environment does have a cooling effect on the non-water bodies of both islands within a certain distance. Under the same climatic and geographical conditions, the spatiotemporal differences of STE between Xiamen Island and Kinmen Island are mainly due to the various urbanization levels, which is reflected in that different urbanization levels correspond to different land cover types in this study. In conclusion, the characteristics and impact factors of STE of inhabited islands are both universal and typical compared to inland cities, suggesting more attention should be paid to the marine environment and urban form for the planning and management of the coastal and island cities in addition to the change in LULC closely related to the urbanization process.

Author Contributions: Methodology, J.Z., C.S. and T.L.; software, J.Z., Y.C. and M.L.; validation, J.Z.; formal analysis, J.Z.; investigation, J.Z.; data curation, J.Z. and Y.Z.; writing—original draft, J.Z.; writing—review and editing, T.L., C.S., M.L., H.Y., Y.H., G.Z. and Y.L.; visualization, J.Z., T.L. and X.Y.; conceptualization, T.L. and C.S.; supervision, T.L.; project administration, T.L.; funding acquisition, T.L. All authors have read and agreed to the published version of the manuscript.

Funding: This research was funded by the Major Special Project—the China High-Resolution Earth Observation System (30-Y30F06-9003-20/22), the International Partnership Program of Chinese Academy of Sciences (Grant No.132C35KYSB20200007), and the National Natural Science Foundation of China (42271299).

Conflicts of Interest: The authors declare no conflict of interest.

Appendix A

Table A1. The image information of Landsat series data and weather parameters of these scenes.

Path/Row	Type	Data	AT *	NSAT * (°C)	RH * (%)	WV * (m/s)
119/43	Landsat TM	20001206	0.66	16.70	73	2.60
		20031215	0.88	14.40	73	2.80
		20061207	0.58	15.80	65	3.00
		20101208	0.89	14.80	65	2.50
	Landsat OLI/TIRS	20141213	0.86	13.90	64	2.90
		20171221	0.92	15.38	61	3.28
		20201111	0.81	21.60	63	3.70

* AT: Atmospheric transmittance; NSAT: Average near-surface air temperature; RH: Relative humidity; WV: Average wind velocity.

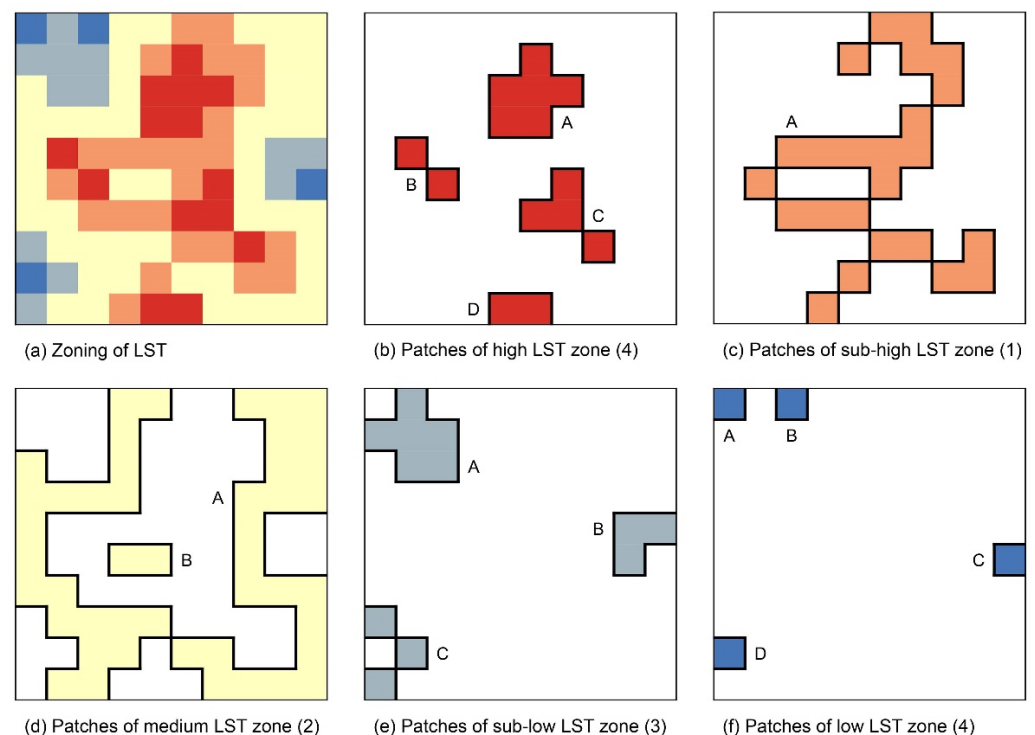


Figure A1. The definition of thermal landscape patches. A patch refers to a part of space that is different in appearance or property from the surrounding environment but has some internal homogeneity and is identified via patch boundaries distinguished by discontinuities in the environmental character states from their surroundings of magnitudes.

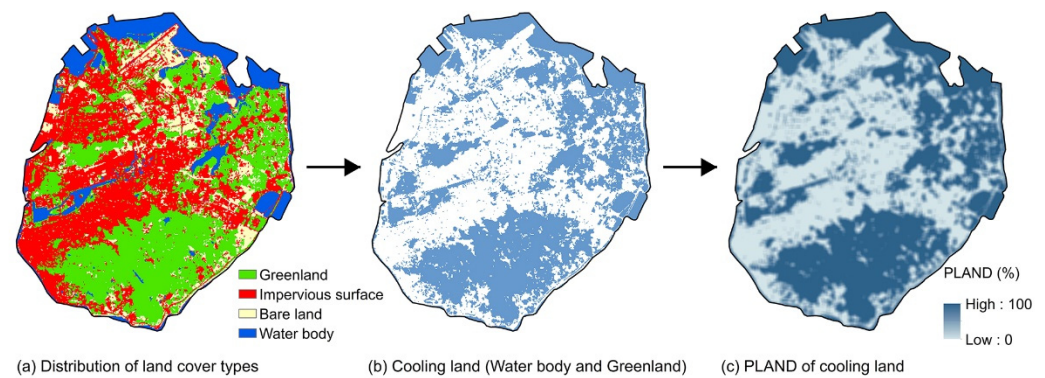


Figure A2. The consistency between the original landscape and land coverage results calculated with PLAND.

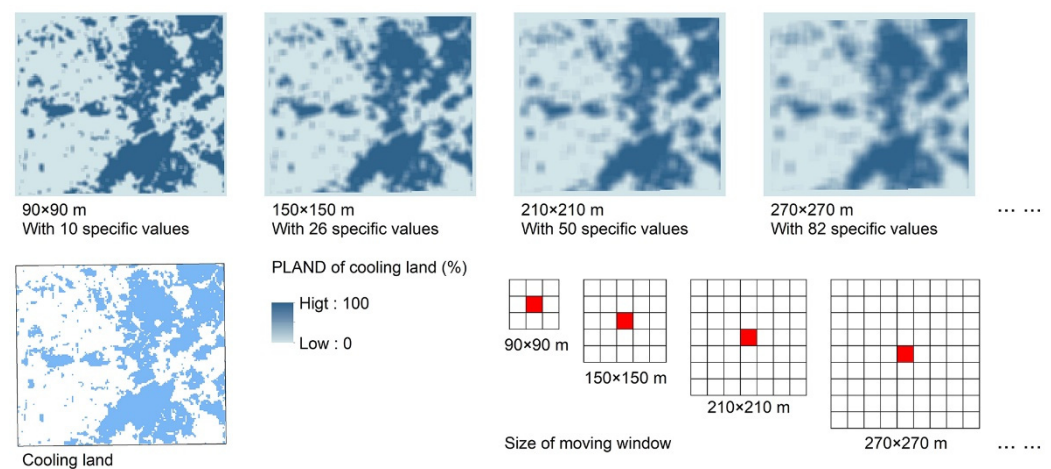


Figure A3. The determination of the moving window size. The side length of the moving window should be an odd multiple of 30 m based on the spatial resolution of remote sensing images, and the continuity of the value of land coverage calculated with small windows (such as 90×90 m and 150×150 m) was too weak to perform the corresponding analysis of LST while the land coverage layer calculated with large windows (270×270 m and above) lost a lot of spatial details that also reduced the accuracy of the analysis. A 210×210 m window was thus selected finally.

References

1. Intergovernmental Panel on Climate Change (IPCC). *Global Warming of 1.5 °C*; Intergovernmental Panel on Climate Change: Geneva, Switzerland, 2018.
2. United Nations (UN). *World Population Prospects 2022: Summary of Results*; United Nations: New York, NY, USA, 2022.
3. United Nations (UN). *World Urbanization Prospects: The 2018 Revision*; United Nations: New York, NY, USA, 2018.
4. Yao, Y.; Chen, X.; Qian, J. Research progress on the thermal environment of the urban surfaces. *Acta Ecol. Sin.* **2018**, *8*, 1134–1147. [[CrossRef](#)]
5. Yuan, F.; Bauer, M.E. Comparison of impervious surface area and normalized difference vegetation index as indicators of surface urban heat island effects in Landsat imagery. *Remote Sens. Environ.* **2007**, *106*, 375–386. [[CrossRef](#)]
6. Voogt, J.A.; Oke, T.R. Thermal remote sensing of urban climates. *Remote Sens. Environ.* **2003**, *86*, 370–384. [[CrossRef](#)]
7. Weng, Q. Thermal infrared remote sensing for urban climate and environmental studies: Methods, applications, and trends. *ISPRS J. Photogramm.* **2009**, *64*, 335–344. [[CrossRef](#)]
8. Laaidi, K.; Zeghnoun, A.; Dousset, B.; Bretin, P.; Vandentorren, S.; Giraudet, E.; Beaudreau, P. The impact of heat islands on mortality in Paris during the August 2003 heat wave. *Environ. Health Perspect.* **2012**, *120*, 254–259. [[CrossRef](#)]
9. Kestens, Y.; Brand, A.; Fournier, M.; Goudreau, S.; Kosatsky, T.; Maloley, M.; Smargiassi, A. Modelling the variation of land surface temperature as determinant of risk of heat-related health events. *Int. J. Health Geogr.* **2011**, *10*, 7. [[CrossRef](#)]
10. Jenerette, G.D.; Harlan, S.L.; Buyantuev, A.; Stefanov, W.L.; Delet-Barreto, J.; Ruddell, B.L.; Myint, S.W.; Kaplan, S.; Li, X. Micro-scale urban surface temperatures are related to land-cover features and residential heat related health impacts in Phoenix, AZ USA. *Landsc. Ecol.* **2015**, *31*, 745–760. [[CrossRef](#)]

11. Mora, C.; Dousset, B.; Caldwell, I.R.; Powell, F.E.; Geronimo, R.C.; Bielecki, C.R.; Counsell, C.W.W.; Dietrich, B.S.; Johnston, E.T.; Louis, L.V.; et al. Global risk of deadly heat. *Nat. Clim. Chang.* **2017**, *7*, 501–506. [[CrossRef](#)]
12. Chen, B.; Xie, M.; Feng, Q.; Li, Z.; Chu, L.; Liu, Q. Heat risk of residents in different types of communities from urban heat-exposed areas. *Sci. Total Environ.* **2021**, *768*, 145052. [[CrossRef](#)]
13. Zhou, D.; Xiao, J.; Bonafoni, S.; Berger, C.; Deilami, K.; Zhou, Y.; Froking, S.; Yao, R.; Qiao, Z.; Sobrino, J. Satellite Remote Sensing of Surface Urban Heat Islands: Progress, Challenges, and Perspectives. *Remote Sens.* **2018**, *11*, 48. [[CrossRef](#)]
14. Rizwan, A.M.; Dennis, L.Y.C.; Liu, C. A review on the generation, determination and mitigation of Urban Heat Island. *J. Environ. Sci.* **2008**, *20*, 120–128. [[CrossRef](#)]
15. Renard, F.; Alonso, L.; Fitts, Y.; Hadjijsif, A.; Comby, J. Evaluation of the Effect of Urban Redevelopment on Surface Urban Heat Islands. *Remote Sens.* **2019**, *11*, 299. [[CrossRef](#)]
16. Sun, L.; Chen, J.; Li, Q.; Huang, D. Dramatic uneven urbanization of large cities throughout the world in recent decades. *Nat. Commun.* **2020**, *11*, 5366. [[CrossRef](#)] [[PubMed](#)]
17. Balsa-Barreiro, J.; Li, Y.; Morales, A.; Pentland, A.S. Globalization and the shifting centers of gravity of world’s human dynamics: Implications for sustainability. *J. Clean. Prod.* **2019**, *239*, 117923. [[CrossRef](#)]
18. Liu, X.; Huang, Y.; Xu, X.; Li, X.; Li, X.; Ciais, P.; Lin, P.; Gong, K.; Ziegler, A.D.; Chen, A.; et al. High-spatiotemporal-resolution mapping of global urban change from 1985 to 2015. *Nat. Sustain.* **2020**, *3*, 564–570. [[CrossRef](#)]
19. Howard, L. *The Climate of London*; London Harvey and Dorton: London, UK, 1833; Volume 2, pp. 1818–1820.
20. Rao, P.K. Remote sensing of urban “heat islands” from an environmental satellite. *Bull. Am. Meteorol. Soc.* **1972**, *53*, 647–648.
21. Zhou, D.; Zhao, S.; Liu, S.; Zhang, L.; Zhu, C. Surface urban heat island in China’s 32 major cities: Spatial patterns and drivers. *Remote Sens. Environ.* **2014**, *152*, 51–61. [[CrossRef](#)]
22. Li, J.; Song, C.; Cao, L.; Zhu, F.; Meng, X.; Wu, J. Impacts of landscape structure on surface urban heat islands: A case study of Shanghai, China. *Remote Sens. Environ.* **2011**, *115*, 3249–3263. [[CrossRef](#)]
23. Ulpiani, G. On the linkage between urban heat island and urban pollution island: Three-decade literature review towards a conceptual framework. *Sci. Total Environ.* **2021**, *751*, 141727. [[CrossRef](#)]
24. Feng, Y.; Du, S.; Myint, S.W.; Shu, M. Do Urban Functional Zones Affect Land Surface Temperature Differently? A Case Study of Beijing, China. *Remote Sens.* **2019**, *11*, 1802. [[CrossRef](#)]
25. Li, X.; Li, W.; Middel, A.; Harlan, S.L.; Brazel, A.J.; Turner, B.L. Remote sensing of the surface urban heat island and land architecture in Phoenix, Arizona: Combined effects of land composition and configuration and cadastral–demographic–economic factors. *Remote Sens. Environ.* **2016**, *174*, 233–243. [[CrossRef](#)]
26. Ma, Q.; Wu, J.; He, C. A hierarchical analysis of the relationship between urban impervious surfaces and land surface temperatures: Spatial scale dependence, temporal variations, and bioclimatic modulation. *Landsc. Ecol.* **2016**, *31*, 1139–1153. [[CrossRef](#)]
27. Li, L.; Zha, Y.; Zhang, J. Spatially non-stationary effect of underlying driving factors on surface urban heat islands in global major cities. *Int. J. Appl. Earth Obs. Geoinf.* **2020**, *90*, 102131. [[CrossRef](#)]
28. Luo, Y. Sustainability Associated Coastal Eco-environmental Problems and Coastal Science Development in China. *Bull. Chin. Acad. Sci.* **2016**, *31*, 1133–1142. [[CrossRef](#)]
29. Lin, T.; Xue, X.; Shi, L.; Gao, L. Urban spatial expansion and its impacts on island ecosystem services and landscape pattern: A case study of the island city of Xiamen, Southeast China. *Ocean Coast. Manag.* **2013**, *81*, 90–96. [[CrossRef](#)]
30. Chi, Y.; Liu, D.; Xing, W.; Wang, J. Island ecosystem health in the context of human activities with different types and intensities. *J. Clean. Prod.* **2021**, *281*, 125334. [[CrossRef](#)]
31. Kier, G.; Kreft, H.; Lee, T.M.; Jetz, W.; Ibsch, P.L.; Nowicki, C.; Mutke, J.; Barthlott, W. A global assessment of endemism and species richness across island and mainland regions. *Proc. Natl. Acad. Sci. USA* **2009**, *106*, 9322–9327. [[CrossRef](#)]
32. Kuo, N.-W.; Chen, P.-H. Quantifying energy use, carbon dioxide emission, and other environmental loads from island tourism based on a life cycle assessment approach. *J. Clean. Prod.* **2009**, *17*, 1324–1330. [[CrossRef](#)]
33. Leoni, B.; Zanotti, C.; Nava, V.; Rotiroti, M.; Stefania, G.A.; Fallati, L.; Soler, V.; Fumagalli, L.; Savini, A.; Galli, P.; et al. Freshwater system of coral inhabited island: Availability and vulnerability (Magoodhoo Island of Faafu Atoll—Maldives). *Sci. Total Environ.* **2021**, *785*, 147313. [[CrossRef](#)]
34. Xiamen Bureau of Statistics, Xiamen Investigation Team of National Bureau of Statistics. *Yearbook of Xiamen Special Economic Zone*; China Statistics Press: Beijing, China, 2021.
35. Directorate General of Budget, Accounting and Statistics (DGBAS) of Executive Yuan. *Statistical Yearbook*; General Statistics Office of the Executive Yuan: Taiwan, China, 2020.
36. Qin, Z.; Karnieli, A.; Berliner, P. A mono-window algorithm for retrieving land surface temperature from Landsat TM data and its application to the Israel-Egypt border region. *Int. J. Remote Sens.* **2001**, *22*, 3719–3746. [[CrossRef](#)]
37. Hu, D.; Qiao, K.; Wang, X.; Zhao, L.; Ji, G. Comparison of Three Single-window Algorithms for Retrieving Land-Surface Temperature with Landsat 8 TIRS Data. *Geomat. Inf. Sci. Wuhan Univ.* **2017**, *42*, 869–876. [[CrossRef](#)]
38. Qin, Z.; Li, W.; Xu, B.; Chen, Z.; Liu, J. The estimation of land surface emissivity for Landsat TM6. *Remote Sens. Nat. Resour.* **2004**, *28–32*, 36, 41. [[CrossRef](#)]
39. Sobrino, J.A.; Jiménez-Muñoz, J.C.; Paolini, L. Land surface temperature retrieval from Landsat TM 5. *Remote Sens. Environ.* **2004**, *90*, 434–440. [[CrossRef](#)]

40. Wang, F.; Qin, Z.; Song, C.; Tu, L.; Karnieli, A.; Zhao, S. An Improved Mono-Window Algorithm for Land Surface Temperature Retrieval from Landsat 8 Thermal Infrared Sensor Data. *Remote Sens.* **2015**, *7*, 4268–4289. [[CrossRef](#)]
41. Chen, S.; Wang, T. Comparison Analyses of Equal Interval Method and Mean-standard Deviation Method Used to Delimitate Urban Heat Island. *J. Geo-Inf. Sci.* **2009**, *11*, 145–150. [[CrossRef](#)]
42. Pal, M.; Mather, P.M. Support vector machines for classification in remote sensing. *Int. J. Remote Sens.* **2005**, *26*, 1007–1011. [[CrossRef](#)]
43. Moran, P.A.P. Notes on Continuous Stochastic Phenomena. *Biometrika* **1950**, *37*, 17–23. [[CrossRef](#)]
44. Ord, J.K.; Getis, A. Local Spatial Autocorrelation Statistics: Distributional Issues and an Application. *Geogr. Anal.* **1995**, *27*, 286–306. [[CrossRef](#)]
45. Mitchell, A. *The ESRI Guide to GIS Analysis*; Esri Press: Redlands, CA, USA, 2005; Volume 2.
46. McGarigal, K. Fragstats Help. 2015. Available online: <https://ibis.geog.ubc.ca/courses/geob479/labs/fragstats.help.4.pdf> (accessed on 20 October 2021).
47. Spearman, C. The proof and measurement of association between two things. *Int. J. Epidemiol.* **2010**, *39*, 1137–1150. [[CrossRef](#)]
48. Kumar, A.; Abirami, S. Aspect-based opinion ranking framework for product reviews using a Spearman’s rank correlation coefficient method. *Inform. Sci.* **2018**, *460–461*, 23–41. [[CrossRef](#)]
49. Kim, S. ppcor: An R Package for a Fast Calculation to Semi-partial Correlation Coefficients. *Commun. Stat. Appl. Methods* **2015**, *22*, 665–674. [[CrossRef](#)]
50. Deilami, K.; Kamruzzaman, M.; Liu, Y. Urban heat island effect: A systematic review of spatio-temporal factors, data, methods, and mitigation measures. *Int. J. Appl. Earth Obs. Geoinf.* **2018**, *67*, 30–42. [[CrossRef](#)]
51. Ciazela, M.; Ciazela, J. Topoclimate Mapping Using Landsat ETM+ Thermal Data: Wolin Island, Poland. *Remote Sens.* **2021**, *13*, 2712. [[CrossRef](#)]
52. Grigoraş, G.; Urişescu, B. Land Use/Land Cover changes dynamics and their effects on Surface Urban Heat Island in Bucharest, Romania. *Int. J. Appl. Earth Obs. Geoinf.* **2019**, *80*, 115–126. [[CrossRef](#)]
53. Hermosilla, T.; Palomar-Vázquez, J.; Balaguer-Beser, Á.; Balsa-Barreiro, J.; Ruiz, L.A. Using street based metrics to characterize urban typologies. *Comput. Environ. Urban Syst.* **2014**, *44*, 68–79. [[CrossRef](#)]
54. Lin, M.; Dong, J.; Jones, L.; Liu, J.; Lin, T.; Zuo, J.; Ye, H.; Zhang, G.; Zhou, T. Modeling green roofs’ cooling effect in high-density urban areas based on law of diminishing marginal utility of the cooling efficiency: A case study of Xiamen Island, China. *J. Clean. Prod.* **2021**, *316*, 128277. [[CrossRef](#)]
55. Hermosilla, T.; Ruiz, L.A.; Recio, J.A.; Balsa-Barreiro, J. Land-use mapping of Valencia city area from aerial images and LiDAR data. In Proceedings of the GEOProcessing 2012: The Fourth International Conference on Advanced Geographic Information Systems, Applications, and Services, Valencia, Spain, 30 January–4 February 2012; pp. 232–237.